Cite as: E. M. Spanton *et al.*, *Science* 10.1126/science.aan8458 (2018).

Observation of fractional Chern insulators in a van der Waals heterostructure

Eric M. Spanton,[1]* Alexander A. Zibrov,[2]* Haoxin Zhou,[2] Takashi Taniguchi,[3] Kenji Watanabe,[3] Michael P. Zaletel,[4] Andrea F. Young[2]†

[1]California Nanosystems Institute, University of California, Santa Barbara, CA 93106, USA. [2]Department of Physics, University of California, Santa Barbara, CA 93106, USA. [3]Advanced Materials Laboratory, National Institute for Materials Science, Tsukuba, Ibaraki 305-0044, Japan. [4]Department of Physics, Princeton University, Princeton, NJ 08544, USA.

*These authors contributed equally to this work.

†Corresponding author. Email: andrea@physics.ucsb.edu

Topologically ordered phases are characterized by long-range quantum entanglement and fractional statistics rather than by symmetry breaking. First observed in a fractionally filled continuum Landau level, topological order has since been proposed to arise more generally at fractional fillings of topologically non-trivial "Chern" bands. Here, we report the observation of gapped states at fractional fillings of Harper-Hofstadter bands arising from the interplay of a magnetic field and a superlattice potential in a bilayer graphene/hexagonal boron nitride heterostructure. We observe phases at fractional filling of bands with Chern indices $\mathcal{C}=-1$, ± 2, and ± 3. Some of these, in $\mathcal{C}=-1$ and $\mathcal{C}=2$ bands, are characterized by fractional Hall conductance—they are "fractional Chern insulators" and constitute an example of topological order beyond Landau levels.

Bands in electronic systems can be classified by their symmetry and topology (*1*). In two dimensions with no symmetries beyond charge conservation, for example, bands are characterized by a topological "Chern" number, $\mathcal{C}$ (*2*). The Chern number determines the Hall conductance contributed by a filled band, which takes quantized integer values, $\sigma_{xy} = t\frac{e^2}{h}$ with $t \in \mathbb{Z}$ (*2*) (here e is the charge of an electron and h is the Planck constant). Systems with an integer number of filled bands with nonzero $\mathcal{C}$ ("Chern bands") thus show a quantized, nonzero Hall conductance, and are known as Chern Insulators (CIs). The first experimental examples of CIs are the integer quantum Hall (IQH) states, observed in isotropic two dimensional electron systems (2DES) subjected to a large magnetic fields (*3*). In the case of IQH, a quantized Hall conductance is observed when an integer number of Landau levels (LLs) are filled, each with $\mathcal{C}=1$.

IQH systems are very nearly translation invariant, in which case t is fixed by the magnetic field B and the electron density n, via $t=\frac{n}{B}\frac{h}{e}$, with some disorder required for the formation of plateaus in the Hall conductance (*4*). Recently, there has been interest in a different class of CIs where continuous translation invariance is strongly broken by a lattice, decoupling the Hall conductance from the magnetic field. CIs in which t is decoupled from $\frac{n}{B}$ have been observed in magnetically doped thin films with strong spin orbit interactions (*5*) and in the Harper-Hofstadter (*2*) bands of graphene subjected to a superlattice potential (*6–8*). Haldane's staggered flux model (*9*), which has nonzero quantized Hall conductance even when the net magnetic field is zero, has been engineered using ultracold atoms in an optical lattice (*10*).

Interactions expand the topological classification of gapped states, allowing the Hall conductance t to be quantized to a rational fraction. By Laughlin's flux-threading argument, an insulator with $t=\frac{p}{q}$ must have a fractionalized excitation with charge $\frac{e}{q}$ (*11*). A fractionally quantized Hall conductance in a bulk insulator is thus a smoking-gun signature of topological order, and fractional quantum Hall (FQH) effects have been observed in partially-filled continuum LLs in a variety of experimental systems (*12–15*). Can a "fractional Chern insulator" (FCI) arise from fractionally filling a more general Chern band (*16*)? Although a FQH effect in a LL may be considered a special case of a FCI, in this work we focus on FCIs that require a lattice for their existence.

The phenomenology of lattice FCIs differs from that of continuum LLs. Chern bands with $\mathcal{C}\neq 1$ can arise, leading to different ground states than are allowed in $\mathcal{C}=1$ LLs. In ad-

dition, unlike LLs, Chern bands generically have a finite, tunable bandwidth that competes with interactions, providing a new setting for the study of quantum phase transitions. Finally, FCIs might be found in experimental systems where Chern bands, but not LLs, are realizable. A large body of theoretical work has begun to investigate these issues (*17–24*).

Here, we report the experimental discovery of FCIs in a bilayer graphene (BLG) heterostructure at high magnetic fields. The requirements to realize an FCI in an experimental system are, first, the existence of a Chern band, and, second, electron-electron interactions strong enough to overcome both disorder and band dispersion. We satisfy these requirements by using a high quality bilayer graphene heterostructure, in which the bilayer is encapsulated between hexagonal boron nitride (hBN) gate dielectrics and graphite top- and bottom gates (Fig. 1, A and B). This geometry was recently demonstrated to significantly decrease disorder, permitting the observation of delicate FQH states (*25*). We generate Chern bands by close rotational alignment (~1°) between the bilayer graphene and one of the two encapsulating hBN crystals. Beating between the mismatched crystal lattices leads to a long-wavelength (~10 nm) moiré pattern that the electrons in the closest layer experience as a periodic superlattice potential (Fig. 1B, (*26*)). At high magnetic fields, the single particle spectrum of an electron in a periodic potential forms the Chern bands of the Hofstadter butterfly (*7–9*). These bands are formally equivalent to Chern bands proposed to occur in zero magnetic field; at any fractional flux, a finite-field lattice model can be converted to an equivalent zero-field model using gauge invariance (*16*).

We measure the penetration field capacitance (*27*) (C_P), which distinguishes between gapped (incompressible) and ungapped (compressible) states (*26*). Figures 1, C-D show C_P measured as a function of B and the electron density, $n \sim n_0 \equiv c\left(v_t + v_b\right)$, where v_t and v_b are the applied top and bottom gate voltages and c denotes the geometric capacitance to either of the two symmetric gates. We use a perpendicular electric field, parameterized by $p_0/c = v_t - v_b$, to localize the charge carriers onto the layer with a superlattice potential, e.g., adjacent to the aligned hBN flake. High C_P features, corresponding to gapped electronic states, are evident throughout the experimentally accessed parameter space (Fig. 1, C and D), following linear trajectories in the $n - B$ plane. We estimate the area of the superlattice unit cell from zero-field capacitance data (*26*), and define the electron density $n_e = Ne/N_S$ and flux density $n_\Phi = N_\Phi / N_S$ per unit cell. Here N_e, N_S, and N_Φ are the number of electrons, superlattice cells, and magnetic flux quanta in the sample, respectively. The trajectories are parameterized by their inverse slope t and n-intercept s in the n-B plane

$$N_e = tN_\Phi + sN_S, \quad n_e = tn_\Phi + s \qquad (1)$$

The Streda (*28*) formula, $t = \frac{\partial n_e}{\partial n_\Phi}|_{N_S} = \frac{h}{e^2}\sigma_{xy}$, shows that the Hall conductance of a gapped phase is exactly t. The invariant $s = \frac{\partial N_e}{\partial N_S}|_{N_{\Phi_0}}$ encodes the amount of charge "glued" to the unit cell, i.e., the charge which is transported if the lattice is dragged adiabatically (*29*). Non-zero s indicates that strong lattice effects have decoupled the Hall conductance from the electron density. Within band theory, the invariants of a gap arise from summing the invariants (Δt_j, Δs_j) of the occupied bands, $(t,s) = \sum_{j \in occ} \left(\Delta t_j, \Delta s_j\right)$; in particular, the Hall conductance t is the sum of the occupied band Chern indices, $\Delta t_j = C_j$.

Based on the properties of t and s, we observe five classes of high-C_P trajectories, each of which correspond to a distinct class of gapped state (Fig. 1, E and F). Free-fermion band gaps must have integer t and s: trajectories with $s = 0$ correspond to gaps between LLs, i.e., IQH states. Trajectories with $s \neq 0$ indicate the formation of the non-LL Chern bands of the Hofstadter butterfly (*6–8*). Trajectories with fractional t or s are beyond the single particle picture and thus indicate interaction-driven gapped phases. The conventional FQH states follow trajectories with fractional t and $s = 0$. Gap trajectories with integer t and fractional s (previously observed in monolayer graphene (*30*)) must be either topologically ordered or have interaction-driven spontaneous symmetry breaking of the superlattice symmetry. The theoretical analysis below suggests the latter case is most likely, so we refer to this class as symmetry-broken Chern insulators (SBCIs). Finally, there are trajectories with fractional t and fractional s, which are the previously unreported class of topologically-ordered FCI phases.

To better understand states with fractional t or s, we first identify the single-particle Chern bands in our experimental data by identifying all integer-t, integer-s gapped states. We focus on adjacent pairs of gapped states with integer (t_L, s_L) and (t_R, s_R), which form the boundaries of a finite range of n_e in which no other single-particle gapped states appear (Fig. 1G). Adding charge to the left gapped state corresponds to filling a Chern band with invariants $(\Delta t, \Delta s) = (t_R - t_L, s_R - s_L)$. From this criterion we find a variety of Chern bands with $\Delta t = \pm 1, \pm 2, \pm 3$ and ± 5 in the experimental data (*26*), each of which appear as a "triangle" between adjacent single-particle gapped states. These Chern bands are observed to obey certain rules expected from the Hofstadter problem: for example, Δt and Δs are always coprime, and Chern bands with Δt always emanate from a flux $n_\Phi^* = p/\Delta t$.

Interaction-driven phases occur at fractional filling v_C of a Chern band, following trajectories

$(t_{vC}, s_{vC}) = (t_L, s_L) + v_C(\Delta t, \Delta s)$. The Chern numbers of the bands in which some of the observed interaction-driven phases appear (Fig. 2, A to C) are denoted schematically in Fig. 2, D to F.

By combining a phenomenological description of the moiré potential with knowledge of orbital symmetry breaking in bilayer graphene (*31*), we are able to construct a single particle model that closely matches the majority of the experimentally observed single-particle Chern bands (*25*). The calculated energy spectra of the bands relevant to Fig. 2, A to C are shown in Fig. 2, G to I. As is clear from the band structure, stable phases at fractional ν_C are not expected within the single particle picture: instead, the encompassing Chern band splits indefinitely into finer Chern bands at lower levels of the fractal butterfly that depend sensitively on n_Φ.

The three columns of Fig. 2 represent instances of three general classes of fractional ν_C states observed in our experiment. Figure 2A shows two gapped states within a $\Delta t = -1$ band at $\nu_C = \frac{1}{3}$ and $\frac{2}{3}$. These gapped states extend from $n_\Phi \approx 0.55$ to at least $n_\Phi \approx 0.8$ (*26*). Both are characterized by fractional t and s, and we identify them as FCI states. As with FQH states, the fractionally quantized Hall conductance implies that the system has a charge $e/3$ excitation (*11*). The fractional s values of these states, being multiples of this fractional charge, do not require broken superlattice symmetry. Gapped states at $\nu_C = 1/3,2/3$ in a $\Delta t = -1$ band are accompanied by comparatively weaker states at $\nu_C = 2/5,3/5$ (Fig. 3B). These fillings match the odd-denominator composite fermion sequence observed for FQH states (Fig. 3C), in agreement with theoretical predictions (*32*).

Figure 2 shows gapped states with fractional s and integer t at $\nu_C = 1/3,2/3$ in a $\Delta t = +3$ band (Fig. 2B) and at $\nu_C = 1/2$ in a $\Delta t = +2$ band (Fig. 2C). Filling a Chern-Δt band to a multiple of $\nu_C = \frac{1}{|\Delta t|}$ corresponds to integer t but fractional s. These states are unlikely to admit a simple interpretation as FCIs; however, we cannot exclude exotic fractionalized states. Absent fractional excitations, a gapped state with fractional $s = \frac{x}{y}$ implies broken superlattice symmetry: the unit cell of such a phase must contain an integral number of electrons, and the smallest such cell contains y superlattice sites. Theoretically, such symmetry breaking is expected to arise spontaneously as a result of electronic interactions, in a lattice analog of quantum Hall ferromagnetism (*33*). A Δt Chern band is similar to a Δt-component LL, but in contrast to an internal spin, translation acts by cyclically permuting the components (*33*–*35*). Spontaneous polarization into one of these components thus leads to a t-fold increase of the unit cell (*33*). The observation of SBCIs is thus analogous to the observation of strong odd-integer IQHEs that break spin-rotational invariance. Some of the "fractional fractal" features recently described in monolayer graphene appear to be consistent with this explanation (*30*).

Finally, we also observe fractional-t states within a $\Delta t = +2$ band (Fig. 3C), for example at $\nu_C = 1/3$ ($t = 8/3$ and $s = -1/3$) and $\nu_C = 1/6$ ($t = 7/3$ and $s = -1/6$). FCIs in Chern-$\Delta t \neq \pm 1$ bands can either preserve or break the underlying lattice symmetry. Symmetry preserving FCIs are expected (*21*, *32*, *36*) at fillings $\nu_C = \frac{m}{2lm\Delta t + 1}$ for integers l,m. The state observed $\nu_C = 1/3$ is consistent with this sequence ($l = 1, m = -1$); in contrast, the weaker state at $\nu_C = 1/6$ is not. For the $\nu_C = 1/6$ state, the observed $t = 7/3$ suggests a fundamental charge of $e/3$. As for SBCIs, the observed $s = -1/6$ implies that each unit cell binds only half a fundamental charge—i.e., the moiré unit cell is doubled and the $\nu_C = 1/6$ state is a "SB-FCI" state. A $\Delta t = 2$ Hofstadter band is similar to a spin degenerate LL, with lattice symmetry taking to place of spin symmetry. In a spin degenerate LL at $\nu_C = 1/6$ (i.e., LL filling $\nu_C = 1/3$) the system spontaneously spin polarizes, forming a single component Laughlin state. In contrast, at $\nu_C = 1/3$ ($\nu_C = 2/3$) the system can either spin polarize (observed only for large Zeeman energy) or form a multicomponent FQH state that preserves spin rotation symmetry. The absence of an obvious analog of the Zeeman effect in our Hofstadter band makes a multicomponent state a more likely candidate for the feature observed at $\nu_C = 2/3$.

To assess the plausibility of FCI and SBCI ground states, we use the infinite density matrix renormalization group (iDMRG) to numerically compute the many body ground state within a minimal model of the BLG (*37*). We first consider Coulomb interactions and a triangular moiré potential of amplitude V_M projected into a BLG $N = 0$ LL (*38*), matching the parameter regime in Fig. 2A (*26*). We focus on $n_\Phi = \frac{2}{3}$ at a density corresponding to $\nu_C = \frac{1}{3}$ filling of the $\Delta t = -1$ band.

If interactions are too weak compared to the periodic potential (as parameterized by V_M/E_C, where $E_C = e^2/(\varepsilon \ell_B)$ is the Coulomb energy, $\ell_B = \sqrt{\frac{\hbar}{eB}}$ is the magnetic length, ε the dielectric constant, and $\hbar$ is the reduced Planck constant, the ground state at $n_\Phi = \frac{2}{3}$ is gapless, corresponding to a partially filled Chern band. If the interactions are too strong, the system forms a Wigner crystal which is pinned by the moiré potential. In the intermediate regime, however, the numerical ground state of this model has a fractional t and s that match

the experiment, and hence is an FCI, with entanglement signatures that indicate a Laughlin-type topological order (*26*). The FCI is stable across a range of V_M/E_C (Fig. 4A) corresponding to $|V_M| \approx 14-38$ meV, consistent with recent (*39*) experiments that suggest $|V_M| \sim 25$ meV. Figure 4B shows that the real-space density of an FCI is strongly modulated by the potential, but preserves all the symmetries of the superlattice.

We next conduct iDMRG calculations to assess the plausibility of the SBCI hypothesis. We focus on the well developed Chern-3 band of Fig. 2, B, E, and H. As a minimal model, we project the moiré and Coulomb interactions into the N = 1 LL of the BLG, fixing V_M = 21 meV and $E_C(B = 17T)$ = 35 meV, and take $n_\Phi = \frac{3}{8}$.

At $\nu_C = \frac{1}{3}$ filling, the electron density indeed exhibits a modulation that spontaneously triples the superlattice unit cell (Fig. 4C). A similar tripling is observed at $\nu_C = \frac{2}{3}$. These are not merely density waves, however, as they have finite (t,s) invariants, in agreement with experiment.

We note that the SBCI states are distinct from a second class of integer-t, fractional-s features, the moiré-pinned Wigner crystals (*30*, *40*). In the latter case, starting from a LL-gap at $t,s = t_L,0$, additional electrons form a Wigner crystal pinned by the moiré; the added electrons are electrically inert, leading to a state at $t,s = t_L,\frac{x}{y}$ that can't be ascribed to fixed ν_C of an encompassing band. These states are thus analogous to reentrant IQH effects, with the moiré playing the role of disorder. In contrast, although the electrons added to the SBCI spontaneously increase the unit cell, they also contribute an integer Hall conductance, which together correspond to some ν_C.

In summary, we find that instead of a self-repeating fractal structure, interactions mix Hofstadter-band wavefunctions to form stable, interaction-driven states at fractional filling of a Chern band. Among these are both symmetry-broken Chern insulators and topologically-ordered fractional Chern insulators, the latter of which constitute a lattice analog of the FQH effect. Lattice engineering can lead to increased experimental control. For example, multicomponent FCI states in higher Chern number bands—as may be responsible for the ν_C = 1/3 feature in Fig. 3C—have been predicted to host non-abelian defects at engineered lattice dislocations (*34*). A pressing experimental question, then, is whether FCI states can be realized in microscopically engineered superlattices.

REFERENCES AND NOTES

1. S. Ryu, A. P. Schnyder, A. Furusaki, A. W. W. Ludwig, Topological insulators and superconductors: Tenfold way and dimensional hierarchy. *New J. Phys.* **12**, 065010 (2010).
2. D. J. Thouless, M. Kohmoto, M. P. Nightingale, M. den Nijs, Quantized Hall conductance in a two-dimensional periodic potential. *Phys. Rev. Lett.* **49**, 405–408 (1982). doi:10.1103/PhysRevLett.49.405
3. K. Klitzing, G. Dorda, M. Pepper, New method for high-accuracy determination of the fine-structure constant based on quantized Hall resistance. *Phys. Rev. Lett.* **45**, 494–497 (1980). doi:10.1103/PhysRevLett.45.494
4. S. M. Girvin, *Topological Aspects of Low Dimensional Systems* (Springer-Verlag, 1999).
5. C.-Z. Chang, J. Zhang, X. Feng, J. Shen, Z. Zhang, M. Guo, K. Li, Y. Ou, P. Wei, L.-L. Wang, Z.-Q. Ji, Y. Feng, S. Ji, X. Chen, J. Jia, X. Dai, Z. Fang, S.-C. Zhang, K. He, Y. Wang, L. Lu, X.-C. Ma, Q.-K. Xue, Experimental observation of the quantum anomalous Hall effect in a magnetic topological insulator. *Science* **340**, 167–170 (2013). doi:10.1126/science.1234414 Medline
6. C. R. Dean, L. Wang, P. Maher, C. Forsythe, F. Ghahari, Y. Gao, J. Katoch, M. Ishigami, P. Moon, M. Koshino, T. Taniguchi, K. Watanabe, K. L. Shepard, J. Hone, P. Kim, Hofstadter's butterfly and the fractal quantum Hall effect in moiré superlattices. *Nature* **497**, 598–602 (2013). doi:10.1038/nature12186 Medline
7. L. A. Ponomarenko, R. V. Gorbachev, G. L. Yu, D. C. Elias, R. Jalil, A. A. Patel, A. Mishchenko, A. S. Mayorov, C. R. Woods, J. R. Wallbank, M. Mucha-Kruczynski, B. A. Piot, M. Potemski, I. V. Grigorieva, K. S. Novoselov, F. Guinea, V. I. Fal'ko, A. K. Geim, Cloning of Dirac fermions in graphene superlattices. *Nature* **497**, 594–597 (2013). doi:10.1038/nature12187 Medline
8. B. Hunt, J. D. Sanchez-Yamagishi, A. F. Young, M. Yankowitz, B. J. LeRoy, K. Watanabe, T. Taniguchi, P. Moon, M. Koshino, P. Jarillo-Herrero, R. C. Ashoori, Massive Dirac fermions and Hofstadter butterfly in a van der Waals heterostructure. *Science* **340**, 1427–1430 (2013). doi:10.1126/science.1237240 Medline
9. F. D. M. Haldane, Model for a quantum Hall effect without Landau levels: Condensed-matter realization of the "parity anomaly". *Phys. Rev. Lett.* **61**, 2015–2018 (1988). doi:10.1103/PhysRevLett.61.2015 Medline
10. G. Jotzu, M. Messer, R. Desbuquois, M. Lebrat, T. Uehlinger, D. Greif, T. Esslinger, Experimental realization of the topological Haldane model with ultracold fermions. *Nature* **515**, 237–240 (2014). doi:10.1038/nature13915 Medline
11. R. B. Laughlin, Anomalous quantum Hall effect: An Incompressible quantum fluid with fractionally charged excitations. *Phys. Rev. Lett.* **50**, 1395–1398 (1983). doi:10.1103/PhysRevLett.50.1395
12. D. C. Tsui, H. L. Stormer, A. C. Gossard, Two-dimensional magnetotransport in the extreme quantum limit. *Phys. Rev. Lett.* **48**, 1559–1562 (1982). doi:10.1103/PhysRevLett.48.1559
13. X. Du, I. Skachko, F. Duerr, A. Luican, E. Y. Andrei, Fractional quantum Hall effect and insulating phase of Dirac electrons in graphene. *Nature* **462**, 192–195 (2009). doi:10.1038/nature08522 Medline
14. K. I. Bolotin, F. Ghahari, M. D. Shulman, H. L. Stormer, P. Kim, Observation of the fractional quantum Hall effect in graphene. *Nature* **462**, 196–199 (2009). doi:10.1038/nature08582 Medline
15. A. Tsukazaki, S. Akasaka, K. Nakahara, Y. Ohno, H. Ohno, D. Maryenko, A. Ohtomo, M. Kawasaki, Observation of the fractional quantum Hall effect in an oxide. *Nat. Mater.* **9**, 889–893 (2010). doi:10.1038/nmat2874 Medline
16. We use "fractional Chern insulator" to denote any non-FQH, topologically ordered state at fractional filling of Chern band, rather than a more restrictive definition requiring the states to occur at zero field.
17. S. A. Parameswaran, R. Roy, S. L. Sondhi, Fractional quantum Hall physics in topological flat bands. *C. R. Phys.* **14**, 816–839 (2013). doi:10.1016/j.crhy.2013.04.003
18. E. J. Bergholtz, Z. Liu, Topological flat band models and fractional Chern insulators. *Int. J. Mod. Phys. B* **27**, 1330017 (2013). doi:10.1142/S021797921330017X
19. A. S. Sørensen, E. Demler, M. D. Lukin, Fractional quantum Hall states of atoms in optical lattices. *Phys. Rev. Lett.* **94**, 086803 (2005). doi:10.1103/PhysRevLett.94.086803 Medline
20. R. N. Palmer, D. Jaksch, High-field fractional quantum Hall effect in optical lattices.

Phys. Rev. Lett. **96**, 180407 (2006). doi:10.1103/PhysRevLett.96.180407 Medline
21. G. Möller, N. R. Cooper, Fractional Chern insulators in Harper-Hofstadter bands with higher Chern number. *Phys. Rev. Lett.* **115**, 126401 (2015). doi:10.1103/PhysRevLett.115.126401 Medline
22. D. N. Sheng, Z.-C. Gu, K. Sun, L. Sheng, Fractional quantum Hall effect in the absence of Landau levels. *Nat. Commun.* **2**, 389 (2011). doi:10.1038/ncomms1380 Medline
23. T. Neupert, L. Santos, C. Chamon, C. Mudry, Fractional quantum Hall states at zero magnetic field. *Phys. Rev. Lett.* **106**, 236804 (2011). doi:10.1103/PhysRevLett.106.236804 Medline
24. N. Regnault, B. A. Bernevig, Fractional Chern insulator. *Phys. Rev. X* **1**, 021014 (2011). doi:10.1103/PhysRevX.1.021014
25. A. A. Zibrov, C. Kometter, H. Zhou, E. M. Spanton, T. Taniguchi, K. Watanabe, M. P. Zaletel, A. F. Young, Tunable interacting composite fermion phases in a half-filled bilayer-graphene Landau level. *Nature* **549**, 360–364 (2017). doi:10.1038/nature23893 Medline
26. See supplementary materials.
27. J. P. Eisenstein, L. N. Pfeiffer, K. W. West, Negative compressibility of interacting two-dimensional electron and quasiparticle gases. *Phys. Rev. Lett.* **68**, 674–677 (1992). doi:10.1103/PhysRevLett.68.674 Medline
28. P. Streda, Theory of quantised Hall conductivity in two dimensions. *J. Phys. C* **15**, L717–L721 (1982). doi:10.1088/0022-3719/15/22/005
29. A. H. MacDonald, Landau-level subband structure of electrons on a square lattice. *Phys. Rev. B* **28**, 6713–6717 (1983). doi:10.1103/PhysRevB.28.6713
30. L. Wang, Y. Gao, B. Wen, Z. Han, T. Taniguchi, K. Watanabe, M. Koshino, J. Hone, C. R. Dean, Evidence for a fractional fractal quantum Hall effect in graphene superlattices. *Science* **350**, 1231–1234 (2015). doi:10.1126/science.aad2102 Medline
31. B. M. Hunt, J. I. A. Li, A. A. Zibrov, L. Wang, T. Taniguchi, K. Watanabe, J. Hone, C. R. Dean, M. Zaletel, R. C. Ashoori, A. F. Young, Direct measurement of discrete valley and orbital quantum numbers in bilayer graphene. *Nat. Commun.* **8**, 948 (2017). doi:10.1038/s41467-017-00824-w Medline
32. A. Kol, N. Read, Fractional quantum Hall effect in a periodic potential. *Phys. Rev. B* **48**, 8890–8898 (1993). doi:10.1103/PhysRevB.48.8890 Medline
33. A. Kumar, R. Roy, S. L. Sondhi, Generalizing quantum Hall ferromagnetism to fractional Chern bands. *Phys. Rev. B* **90**, 245106 (2014). doi:10.1103/PhysRevB.90.245106
34. M. Barkeshli, X.-L. Qi, Topological nematic states and non-Abelian lattice dislocations. *Phys. Rev. X* **2**, 031013 (2012). doi:10.1103/PhysRevX.2.031013
35. Y.-L. Wu, N. Regnault, B. A. Bernevig, Bloch model wave functions and pseudopotentials for all fractional Chern insulators. *Phys. Rev. Lett.* **110**, 106802 (2013). doi:10.1103/PhysRevLett.110.106802 Medline
36. A. Sterdyniak, C. Repellin, B. A. Bernevig, N. Regnault, Series of Abelian and non-Abelian states in $C > 1$ fractional Chern insulators. *Phys. Rev. B* **87**, 205137 (2013). doi:10.1103/PhysRevB.87.205137
37. M. P. Zaletel, R. S. K. Mong, F. Pollmann, E. H. Rezayi, Infinite density matrix renormalization group for multicomponent quantum Hall systems. *Phys. Rev. B* **91**, 045115 (2015). doi:10.1103/PhysRevB.91.045115
38. X. Chen, J. R. Wallbank, M. Mucha-Kruczyński, E. McCann, V. I. Fal'ko, Zero-energy modes and valley asymmetry in the Hofstadter spectrum of bilayer graphene van der Waals heterostructures with hBN. *Phys. Rev. B* **94**, 045442 (2016). doi:10.1103/PhysRevB.94.045442
39. M. Lee, J. R. Wallbank, P. Gallagher, K. Watanabe, T. Taniguchi, V. I. Fal'ko, D. Goldhaber-Gordon, Ballistic miniband conduction in a graphene superlattice. *Science* **353**, 1526–1529 (2016). doi:10.1126/science.aaf1095 Medline
40. A. M. DaSilva, J. Jung, A. H. MacDonald, Fractional Hofstadter states in graphene on hexagonal boron nitride. *Phys. Rev. Lett.* **117**, 036802 (2016). doi:10.1103/PhysRevLett.117.036802 Medline
41. L. Wang, I. Meric, P. Y. Huang, Q. Gao, Y. Gao, H. Tran, T. Taniguchi, K. Watanabe, L. M. Campos, D. A. Muller, J. Guo, P. Kim, J. Hone, K. L. Shepard, C. R. Dean, One-dimensional electrical contact to a two-dimensional material. *Science* **342**, 614–617 (2013). doi:10.1126/science.1244358 Medline
42. R. K. Goodall, R. J. Higgins, J. P. Harrang, Capacitance measurements of a quantized two-dimensional electron gas in the regime of the quantum Hall effect. *Phys. Rev. B* **31**, 6597–6608 (1985). doi:10.1103/PhysRevB.31.6597 Medline
43. P. G. Harper, Single band motion of conduction electrons in a uniform magnetic field. *Proc. Phys. Soc. A* **68**, 874–878 (1955). doi:10.1088/0370-1298/68/10/304
44. M. Ya. Azbel, Energy spectrum of a conduction electron in a magnetic field. *Sov. Phys. JETP* **19**, 634–645 (1964).
45. D. R. Hofstadter, Energy levels and wave functions of Bloch electrons in rational and irrational magnetic fields. *Phys. Rev. B* **14**, 2239–2249 (1976). doi:10.1103/PhysRevB.14.2239
46. D. Langbein, The tight-binding and the nearly-free-electron approach to lattice electrons in external magnetic fields. *Phys. Rev.* **180**, 633–648 (1969). doi:10.1103/PhysRev.180.633
47. D. Pfannkuche, R. R. Gerhardts, Theory of magnetotransport in two-dimensional electron systems subjected to weak two-dimensional superlattice potentials. *Phys. Rev. B* **46**, 12606–12626 (1992). doi:10.1103/PhysRevB.46.12606 Medline
48. R. R. Gerhardts, D. Weiss, U. Wulf, Magnetoresistance oscillations in a grid potential: Indication of a Hofstadter-type energy spectrum. *Phys. Rev. B* **43**, 5192–5195 (1991). doi:10.1103/PhysRevB.43.5192 Medline
49. T. Schlösser, K. Ensslin, J. P. Kotthaus, M. Holland, Internal structure of a Landau band induced by a lateral superlattice: A glimpse of Hofstadter's butterfly. *Europhys. Lett.* **33**, 683 (1996). doi:10.1209/epl/i1996-00399-6
50. M. Hafezi, A. S. Sørensen, E. Demler, M. D. Lukin, Fractional quantum Hall effect in optical lattices. *Phys. Rev. A* **76**, 023613 (2007). doi:10.1103/PhysRevA.76.023613
51. G. Möller, N. R. Cooper, Composite fermion theory for bosonic quantum Hall states on lattices. *Phys. Rev. Lett.* **103**, 105303 (2009). doi:10.1103/PhysRevLett.103.105303 Medline
52. A. Sterdyniak, N. Regnault, G. Moller, Particle entanglement spectra for quantum Hall states on lattices. *Phys. Rev. B* **86**, 165314 (2012). doi:10.1103/PhysRevB.86.165314
53. T. Scaffidi, S. H. Simon, Exact solutions of fractional Chern insulators: Interacting particles in the Hofstadter model at finite size. *Phys. Rev. B* **90**, 115132 (2014). doi:10.1103/PhysRevB.90.115132
54. F. Harper, S. H. Simon, R. Roy, Perturbative approach to flat Chern bands in the Hofstadter model. *Phys. Rev. B* **90**, 075104 (2014). doi:10.1103/PhysRevB.90.075104
55. C. H. Lee, R. Thomale, X.-L. Qi, Pseudopotential formalism for fractional Chern insulators. *Phys. Rev. B* **88**, 035101 (2013). doi:10.1103/PhysRevB.88.035101
56. D. Bauer, T. S. Jackson, R. Roy, Quantum geometry and stability of the fractional quantum Hall effect in the Hofstadter model. *Phys. Rev. B* **93**, 235133 (2016). doi:10.1103/PhysRevB.93.235133
57. D. Pfannkuche, A. H. MacDonald, Quantum Hall effect of interacting electrons in a periodic potential. *Phys. Rev. B* **56**, R7100–R7103 (1997). doi:10.1103/PhysRevB.56.R7100
58. Z. Papić, D. A. Abanin, Topological phases in the zeroth Landau level of bilayer graphene. *Phys. Rev. Lett.* **112**, 046602 (2014). doi:10.1103/PhysRevLett.112.046602 Medline
59. I. P. McCulloch, arXiv:0804:2509 (2008).
60. H. Li, F. D. M. Haldane, Entanglement spectrum as a generalization of entanglement entropy: Identification of topological order in non-Abelian fractional quantum Hall effect states. *Phys. Rev. Lett.* **101**, 010504 (2008). doi:10.1103/PhysRevLett.101.010504 Medline
61. M. P. Zaletel, R. S. Mong, F. Pollmann, Flux insertion, entanglement, and quantized responses. *J. Stat. Mech.* **2014**, P10007 (2014). doi:10.1088/1742-5468/2014/10/P10007
62. F. Pollmann, S. Mukerjee, A. M. Turner, J. E. Moore, Theory of finite-entanglement scaling at one-dimensional quantum critical points. *Phys. Rev. Lett.* **102**, 255701 (2009). doi:10.1103/PhysRevLett.102.255701 Medline

ACKNOWLEDGMENTS

The authors acknowledge discussions with Maissam Barkeshli, Andrei Bernevig, Cory Dean, and Roger Mong and experimental assistance from Jan Jaroszynski and Matthew Yankowitz. **Funding:** The numerical simulations were performed on computational resources supported by the Princeton Institute for Computational Science and Engineering using iDMRG code developed with Roger Mong and the TenPy Collaboration. EMS acknowledges the support of the Elings Fellowship. K.W. and T.T. acknowledge support from the Elemental Strategy Initiative

conducted by the MEXT, Japan and JSPS KAKENHI Grant Number JP15K21722. Measurements were performed at the National High Magnetic Field Laboratory, which is supported by National Science Foundation Cooperative Agreement No. DMR-1157490 and the State of Florida. Magnetocapacitance measurements were funded by the NSF under DMR-1654186. A portion of the nanofabrication and transport measurements were funded by ARO under proposal 69188PHH. AFY acknowledges the support of the David and Lucile Packard Foundation.
Author contributions: E.M.S. and A.A.Z contributed equally to this manuscript. A.A.Z., E.M.S., and H.Z. performed the measurements. S.Z. fabricated the device. T.T. and K.W. provided hexagonal boron nitride single crystals. M.P.Z. performed calculations. E.M.S., A.A.Z., M.P.Z., and A.F.Y. wrote the manuscript with input from all coauthors. **Competing interests:** None declared. **Data and materials availability:** Experimental data files are available from the Open Science Framework at http://osf.io/7qckf/.

SUPPLEMENTARY MATERIALS

www.sciencemag.org/cgi/content/full/science.aan8458/DC1
Materials and Methods
Supplementary Text
Figs. S1 to S14
Tables S1 and S2
References (*41*–*62*)

26 May 2017; accepted 13 February 2018
Published online 1 March 2018
10.1126/science.aan8458

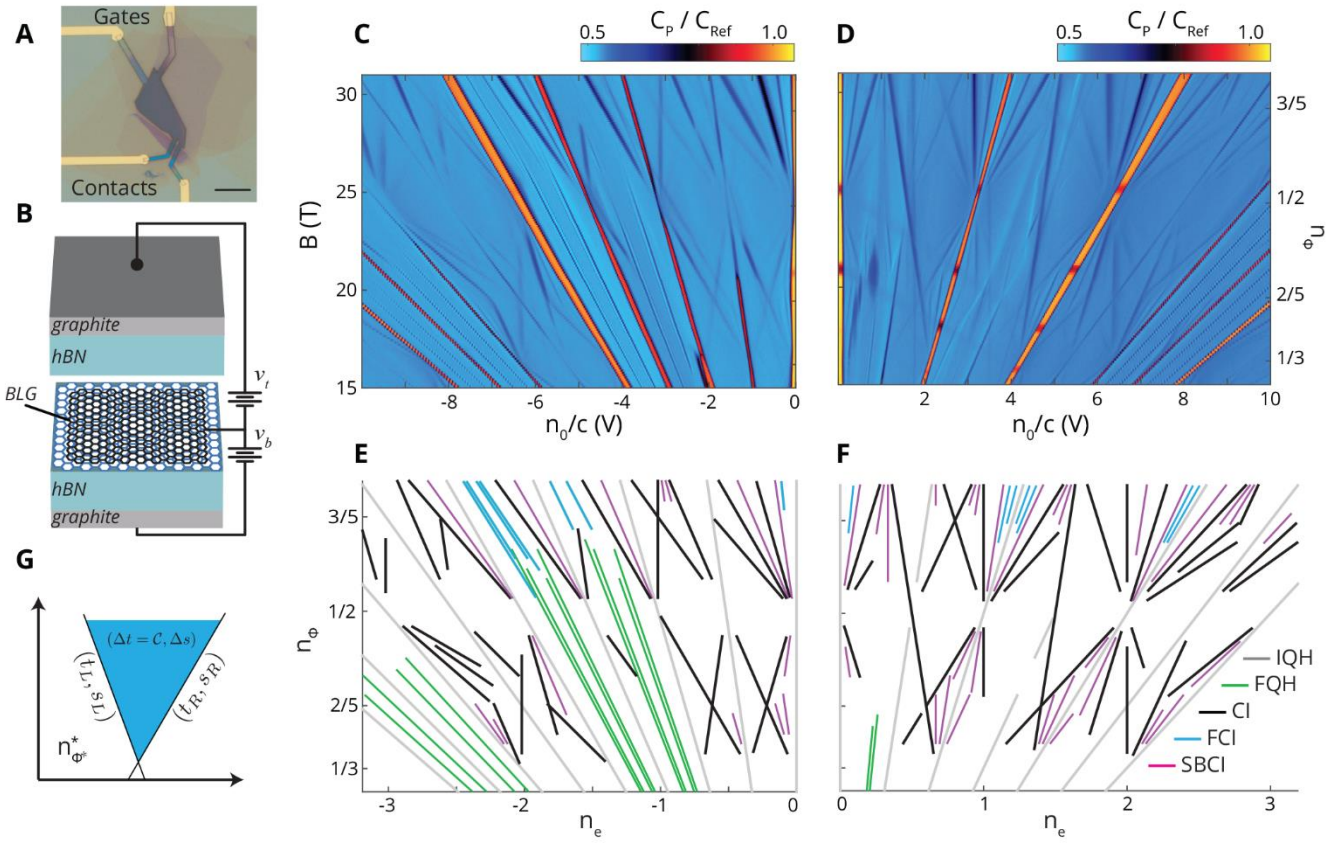

Fig. 1. Magnetocapacitance in a high-quality bilayer graphene moiré superlattice device. (**A**) Optical micrograph of the device. Scale bar is 10 μm. (**B**) Schematic of the device, with top and bottom graphite gates at potential v_t,v_b. A moiré potential is induced by alignment of the graphene bilayer with one of the encapsulating hBN crystals. (**C**) Penetration field capacitance (C_P) as a function of density $n_e \sim n_0 \equiv c\left(v_t + v_b\right)$ and magnetic field B for $n_0 < 0$. T = 300 mK, and C_{Ref} is a reference capacitance. A large electric field p_0/c = $(v_t - v_b)$ = 16V is applied to force the valence electrons onto the top layer, which is in contact with the aligned hBN. (**D**) C_P for $n_0 > 0$ with $v_t - v_b$ = –16 V at T = 300 mK. (**E** and **F**) Linear gap trajectories observed in (C-D) parameterized by $n_e = t \cdot n_\Phi + s$. n_Φ and n_e are the magnetic flux quanta and number of electrons per moiré unit cell, respectively. $n_\Phi \equiv \frac{\sqrt{3}\lambda^2 B}{2\Phi_0} = 1/2$ when B = 24.3 T and n_e = 1 when n_0/c = 3.1V. Five trajectory classes are distinguished by color: Integer quantum Hall (gray, s = 0, $t \in \mathbb{Z}$), fractional quantum Hall (green, s = 0, t fractional), Hofstadter Chern insulators (black, $s, t \in \mathbb{Z}$, $s \neq 0$), symmetry-broken Chern insulators (magenta, fractional s, $t \in \mathbb{Z}$) and fractional Chern insulators (cyan, fractional s,t). (**G**) Schematic of a (Δt,Δs) Chern band (see main text).

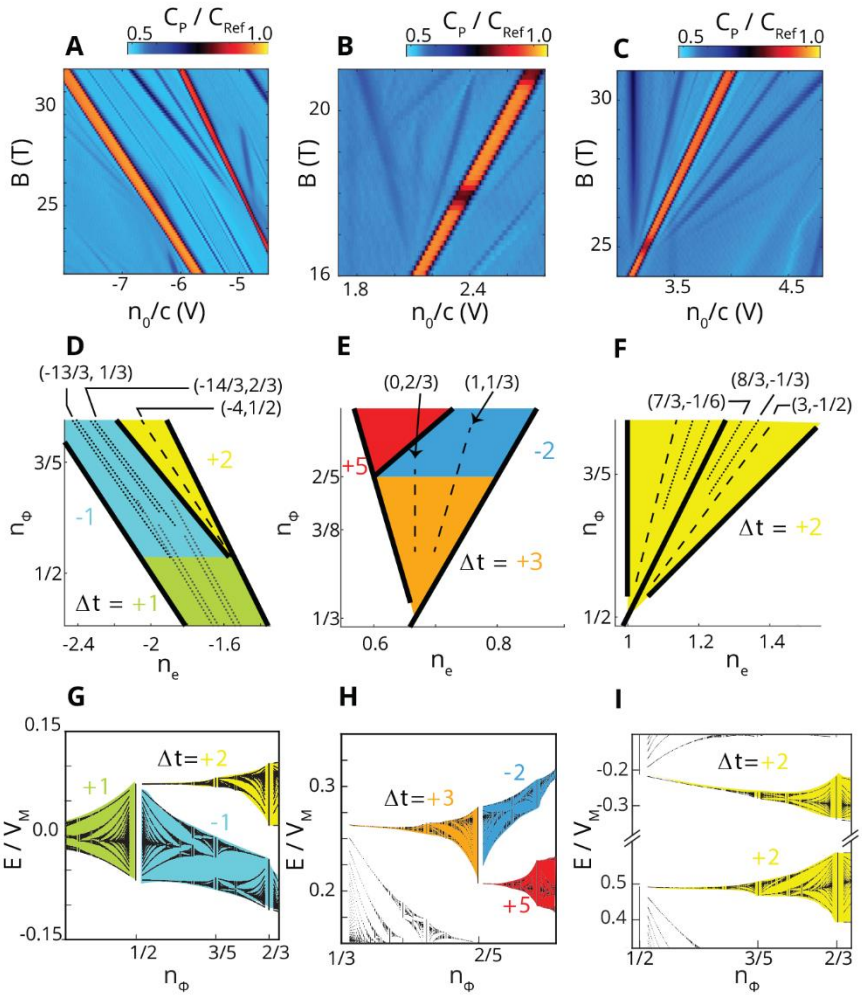

Fig. 2. Interaction driven states at partial Chern-band filling. (A to C) Details of Fig. 1, C and D showing (A) FCI states in a $\Delta t = -1$ band, (B) SBCI states in a $\Delta t = +3$ band, and (C) FCI and SBCI states in $\Delta t = 2$ bands. (D) Schematic of (A). FCI states (black dotted lines) with $(t,s) = (-13/3,1/3)$, $(-22/5,2/5)$, $(-23/5,3/5)$, and $(-14/3,2/3)$ occur at fractional filling of a $\Delta t = -1$ band (light blue). FQH states (gray dotted lines) occur at fractional filling of a conventional LL ($\Delta t = +1$, green) at low fields. (E) Schematic of (B). SBCI states (dashed lines) at and occur at 1/3 and 2/3 fractional filling of a $\Delta t = 3$ band (orange). (F) Schematic of (C). Both FCI and SBCI states (dotted and dashed lines) occur in the $\Delta t = 2$ bands (G) Calculated Hofstadter energy spectrum (*25*) in the regime of (A), matching the observation that the LL splits into $\mathcal{C} = -1, 2$ bands. (H) Calculated Hofstadter spectrum in the regime of (B), matching the observed splitting of a $\mathcal{C} = 3$ band into $\mathcal{C} = 5, -2$ bands. (I) Calculated Hofstadter spectrum in the regime of (C). The IQH gap at $\nu = 2$ separates the two single-particle bands and is much larger than ν_M.

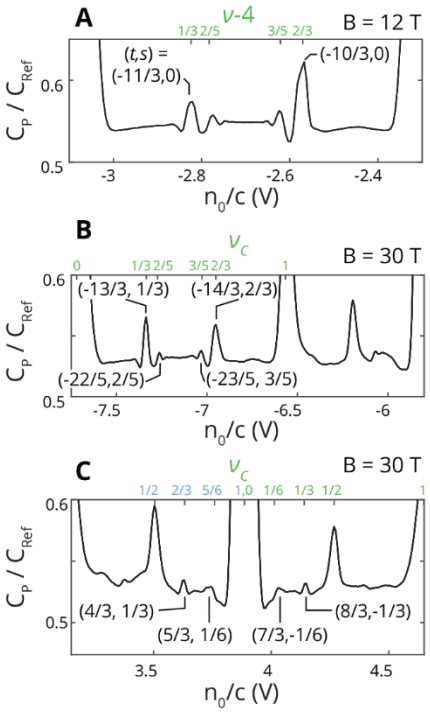

Fig. 3. Line cuts of C_P comparing FCI and FQH states. (**A**) Line cut C_P of vs. n_0/c (bottom axis) and Chern band filling factor (ν_C, top axis). The data are averaged over p_0/c ~ 1.0 – 4.0V at B = 12 T, showing FQH states in a conventional LL. At low fields, the effective moiré potential is weak, and FQH states are observed at filling factors $\nu - 4 = 1/3,2/3$ as well as 2/5,3/5 of the $\Delta t = +1$ LL. (**B**) Line cut averaged over p_0/c ~ 4.0 – 14.0V at B = 30 T, showing FCI in the a $\Delta t = -1$ band (also shown in Fig. 2A). Weaker features appear at $\nu_C = 2/5,3/5$, similar to the composite fermion sequence in (A). (**C**) Line cut averaged over p_0/c ~ –14.0 to – 9.0V at B = 30 T, showing FCI in two $\Delta t = 2$ bands (also shown in Fig. 2C). Blue and green values indicate filling of two distinct bands. The relative strength of the $\nu_C = 1/3$ state compared to the $\nu_C = 1/6$ state in the right $\Delta t = 2$ band is consistent with the former preserving the lattice symmetry.

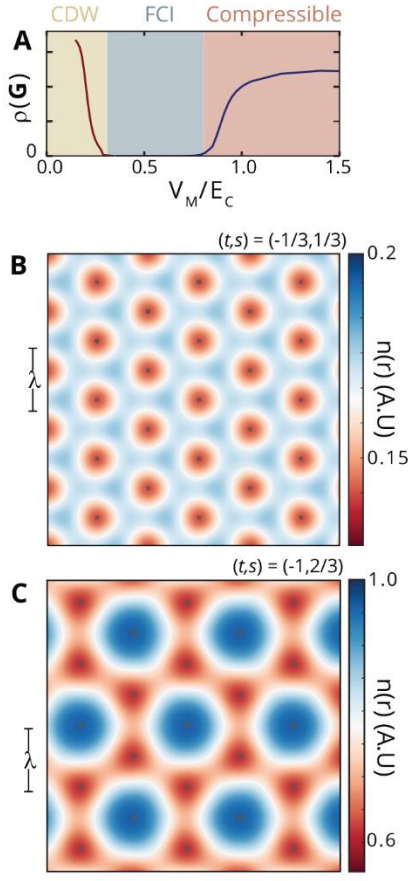

Fig. 4. iDMRG calculations showing the stability of FCI and SBCI states. (**A**) Calculated iDMRG phase diagram at $\nu_C = 1/3$ filling of the $\Delta t = -1$ band shown in Fig. 2, A, D, and G $(n_\Phi = 2/3)$. V_M is the moiré potential amplitude, E_C is the Coulomb energy, and $\rho(\mathbf{G})$ is the charge density at Bragg vector $\mathbf{G}$. The FCI competes with two other phases: a charge density wave (CDW) at low V_M, and a compressible phase at high V_M. The competing phases are diagnosed by symmetry breaking density waves at wavevector $\mathbf{G} = \mathbf{G}_0/3$ (red) and $\mathbf{G} = \mathbf{G}_0/2$ (blue), where $\mathbf{G}_0$ is a reciprocal vector of the moiré (*25*). (**B**) Calculated real-space electron density $n(r)$ of the FCI found in (A). $n(r)$ preserves the symmetry of the moiré potential, whose periodicity is indicated by the gray circles. Here V_M/E_C = 0.7. (**C**) Calculated real-space electron density $n(r)$ at $\nu_C = \frac{2}{3}$ filling of the $\Delta t = 3$ band shown in Fig. 2, B, E, and H $(n_\Phi = 3/8)$. The result is consistent with an SBCI phase; $(t,s) = (-1,2/3)$, and $n(r)$ spontaneously triples the unit cell of the underlying moiré potential, indicated by gray circles. Here $V_M/E_C = 0.6$ and $\Theta_M = \pi/8$.

Observation of fractional Chern insulators in a van der Waals heterostructure

Eric M. Spanton, Alexander A. Zibrov, Haoxin Zhou, Takashi Taniguchi, Kenji Watanabe, Michael P. Zaletel and Andrea F. Young

published online March 1, 2018